Journal of Physics and Chemistry of Solids 170 (2022) 110928

Contents lists available at ScienceDirect

Journal of Physics and Chemistry of Solids

journal homepage: www.elsevier.com/locate/jpcs

Structural characterization, continuous-wave optically stimulated luminescence, and correlation between thermoluminescence and EPR of Ce-doped $Ca_2Al_2SiO_7$ phosphor synthesized by a solid-state reaction method

Nilo F. Cano [b,*], Amador J. Gonsalez-Vasquez [a], T.K. Gundu Rao [a], Klinton V. Turpo-Huahuasoncco [a], Edwar A. Canaza-Mamani [a], Alejandro H. Lopez-Gonzales [a], Henry S. Javier-Ccallata [a], Jorge S. Ayala-Arenas [a], René R. Rocca [b], Noemi B. Silva-Carrera [c], José F.D. Chubaci [c], Shigueo Watanabe [c]

[a] Escuela Profesional de Física, Facultad de Ciencias Naturales y Formales, Universidad Nacional de San Agustín de Arequipa (UNSA), Av. Independencia S/N, Arequipa, Peru
[b] Instituto do Mar, Universidade Federal de São Paulo, Rua Doutor Carvalho de Mendonça, 144, CEP, 11070-100, Santos, SP, Brazil
[c] Instituto de Física, Universidade de São Paulo, Rua do Matão, Travessa R, 187, CEP, 05508-090, São Paulo, SP, Brazil

ARTICLE INFO

Keywords:
Calcium aluminosilicate ($Ca_2Al_2SiO_7$)
Thermoluminescence
Optically stimulated luminescence
Electron paramagnetic resonance
Defect centers

ABSTRACT

A calcium aluminum silicate ($Ca_2Al_2SiO_7$) phosphor doped with different concentrations of cerium has been prepared by a solid-state reaction method. From X-ray diffraction (XRD) data and using the Rietveld refinement method, the phase, structure, and average crystalline size have been determined. Luminescence emissions have been investigated by optically stimulated luminescence (OSL) and thermoluminescence (TL) methods. TL studies reveal a broad peak centered at 220 °C with an emission band at 410 nm. The TL intensity of a sample doped with 0.1 mol% Ce proved to be 115 times stronger than that of an undoped sample. Electron paramagnetic resonance (EPR) has been utilized to detect the defect centers responsible for the TL process in Ce-doped $Ca_2Al_2SiO_7$ phosphor. The observed EPR spectrum results from a superposition of three defect centers. Center I with a *g*-value of 2.0090 is assigned to an O^- ion and exhibits hyperfine interaction with a nearby nucleus with spin 3/2. This center relates to the TL peak at 220 °C. Center II with an isotropic *g*-value of 2.0073 is also ascribed to an O^- ion and correlates with the dominant 220 °C TL peak. Center III has a *g*-value of 2.0076 and is identified as an F^+ center (singly-ionized oxygen vacancy).

1. Introduction

Luminescent materials, both natural and synthetic, are widely used in radiation dosimetry [1,2]. The luminescent intensity is proportional to the amount of energy absorbed, i.e., the dose of radiation to which the material has been exposed. Dose measurements can be performed by optically stimulated luminescence (OSL) and thermoluminescence (TL) techniques and with various materials. The defect centers created by ionizing radiation are responsible for both OSL and TL [3,4].

Calcium aluminum silicate ($Ca_2Al_2SiO_7$) is a material that displays high thermal and chemical stability, and is amenable to the incorporation of dopants, such as rare earths. This material has several applications, including the preparation of photonic sources in lasers [5–8], light-emitting diodes [9], luminescent phosphors, and scintillators [10–18]. In addition, it can be used in piezoelectric sensors [19], and in cements for use in dentistry [20].

The use of this type of material in the preparation of light-emitting sources is associated with the formation of defects in its crystalline structure through the insertion of dopants. Simondi-Teisseire et al. [5] and Lejus et al. [6] showed that single crystals of calcium aluminum silicate doped with Er^{3+}, Yb^{3+}, or Nd^{3+} have wide emission ranges and are useful for the preparation of light emitters with applications in laser materials. On the other hand, this material shows emission in the red-light region when it is doped with Eu^{3+} [7,14]. Jiao and Wang [9]

* Corresponding author. Instituto do Mar, Universidade Federal de São Paulo, Rua Doutor Carvalho de Mendonça, 144, CEP, 11070-100, Santos, SP, Brazil
E-mail addresses: nilo.cano@unifesp.br (N.F. Cano), kturpoh@unsa.edu.pe (K.V. Turpo-Huahuasoncco).

https://doi.org/10.1016/j.jpcs.2022.110928
Received 9 April 2022; Received in revised form 21 July 2022; Accepted 22 July 2022
Available online 31 July 2022

showed that it is possible to use this material to obtain white-light emitters when combined with Ce^{3+} and Tb^{3+}. Yamaga et al. [11] reported phosphorescence properties when Ca and Al silicate is doped with Ce^{3+}. Wang et al. [10] showed that crystalline systems of Ca and Al silicate doped with Ce^{3+} and Mn^{2+} exhibit long-live luminescence property.

Recently, Son et al. [8] synthesized pure $Ca_2Al_2SiO_7$ crystals doped with rare-earth ions (Ce^{3+}, Sm^{3+}, Dy^{3+}, Eu^{3+}, Tb^{3+}) for optical applications by a solid-state reaction method. They observed that the Ce^{3+} -doped sample exhibited a wide emission range, while the samples doped with Dy^{3+}, Tb^{3+}, Sm^{3+}, or Eu^{3+} showed narrow emission lines, characterized by transitions in the 4f electron configuration.

Tiwari et al. [15,16] synthesized Ce^{3+} -doped $Ca_2Al_2SiO_7$ samples by an assisted combustion method, and then studied their mechanoluminescence, thermoluminescence and photoluminescence properties. They showed this Ce^{3+} -doped material to be quite promising for thermoluminescence UV dosimetry applications. According to Tiwari et al. [15,16], $Ca_2Al_2SiO_7$ exhibits a longer duration of light emission at high initial intensity due to a higher probability of release of trapped charge carriers.

Sharma et al. [17] synthesized $CaSrAl_2SiO_7$ doped with different concentrations of Dy^{3+} by a solid-state reaction method. When excited at 350 nm, these samples showed intense emission bands in the blue and yellow regions. The combination of these two bands gives rise to white light. In addition, these authors studied the TL properties of the materials when exposed to UV light irradiation. The TL intensity increased with irradiation time, with characteristic peaks due to Dy^{3+} with light emission at 480 and 580 nm. These results suggested that the sample may be useful in UV dosimetry applications.

Kodama et al. [21] produced single crystals of $Ca_2Al_2SiO_7$ doped with Ce^{3+} using the Czocharlski technique. They showed that this material has a long light emission and can be used in solid-state laser materials. In addition, electrons can recombine with thermally stable hole centers due to Ce^{3+}, leading to energy emission in the UV region.

In recent years, a variety of natural and synthetic silicates have been investigated to elucidate the role of defects formed with γ-irradiation, as well as the role of dopants in TL emission processes [22–27].

Electron paramagnetic resonance (EPR) is one of the most sensitive and informative techniques used for the detection and identification of ionizing-radiation-induced defects formed in the crystal lattice of a material. The results obtained by this technique can be correlated with those obtained by other experimental techniques, such as TL. As a result, it is possible to identify defect centers and establish their role in TL light emission.

In the present study, the OSL, TL and EPR properties of Ce^{3+} -doped calcium aluminum silicate synthesized by the solid-state reaction method have been investigated. Thermoluminescence detected after γ-irradiation in combination with EPR has allowed determination of the defect centers involved during TL emission of this phosphor.

2. Materials and methods

Pure $Ca_2Al_2SiO_7$ as well as samples doped with Ce^{3+} ions (Ce^{3+} = 0.10, 0.25, 0.50, 0.75, 1.00, and 2.00 mol%) were prepared by a solid-state synthesis method. All the chemicals were of analytical grade with 99.9% purity. For the synthesis SiO_2, Al_2O_3, $CaCO_3$, and CeO_2 precursors were used, and H_3BO_3 was added as a flux. Precursors in the appropriate stoichiometric ratio were mixed and homogenized in a mill using alumina spheres for 4 h. The crushed samples were then transferred to alumina crucibles and heated in air at 1400 °C for 5 h in a Nabertherm furnace. They were then allowed to cool slowly in the furnace. Thereafter, the samples were again crushed and subjected to heat treatment at 1300 °C for 2 h. Finally, each sample was crushed for X-ray diffraction (XRD), OSL, TL and EPR measurements.

The structures of the as-prepared samples were analyzed by powder XRD using a Rigaku MiniFlex 600 diffractometer operating at 40 kV and 15 mA, employing Cu-*K*α-radiation. The XRD measurements were made over the Bragg angle range $15° \leq 2\theta \leq 60°$ with a step size of 0.005° and a scan rate of 0.6 s at room temperature.

For TL measurements, powder samples were exposed to γ-rays from a ^{60}Co source for various exposures (1–100 Gy) at room temperature. The dose rate for γ-ray irradiation was 0.64 kGy/h. TL glow curves were recorded on a Harshaw TLD reader for light detection by taking 4.0 ± 0.1 mg of sample each time. They were recorded under nitrogen atmosphere at a heating rate of 4 °C/s. Each point in the glow curve represents an average of five readings.

OSL measurements were performed with a Risø TL/OSL automated reader, model DA-20 equipped with a $^{90}Sr/^{90}Y$ β-source with a dose rate of 0.081 Gy/s. For OSL measurements, the samples were stimulated in continuous-wave (CW) mode using 470 nm light at 80 mW/cm^2, and the OSL light was detected for 40 s at 120 °C in the UV region using a 7.5 mm Hoya U-340 optical filter. All OSL measurements were performed using a single aliquot of the same mass. TL emission spectra were measured by connecting a monochromator to the Risø TL/OSL automated reader.

EPR measurements were carried out using a Freiberg Instruments MiniScope EPR spectrometer Model 5500 with a microwave frequency of 9.42 GHz. EPR spectra were obtained at room temperature (25 °C). The samples were irradiated with a γ-dose of 10–500 Gy before recording their EPR spectra. Recording parameters were a central field of 337 mT, a modulation amplitude of 0.2 mT, a modulation frequency of 100 kHz, and a microwave power of 20 mW. EPR intensity was measured by peak-to-peak amplitude. A standard sample of 2,2-diphenyl-1-picrylhydrazyl (DPPH) was used to calibrate the *g*-factor of the signal. Powder samples irradiated at room temperature with ^{60}Co γ-radiation were placed in quartz capillary tubes, which were in turn placed inside the EPR cavity, using a mass of 150.0 ± 0.1 mg. EPR spectra of the irradiated samples were also recorded at different annealing temperatures in the range 50–280 °C.

3. Results and discussion

Fig. 1a shows the XRD spectra of the undoped $Ca_2Al_2SiO_7$ and the

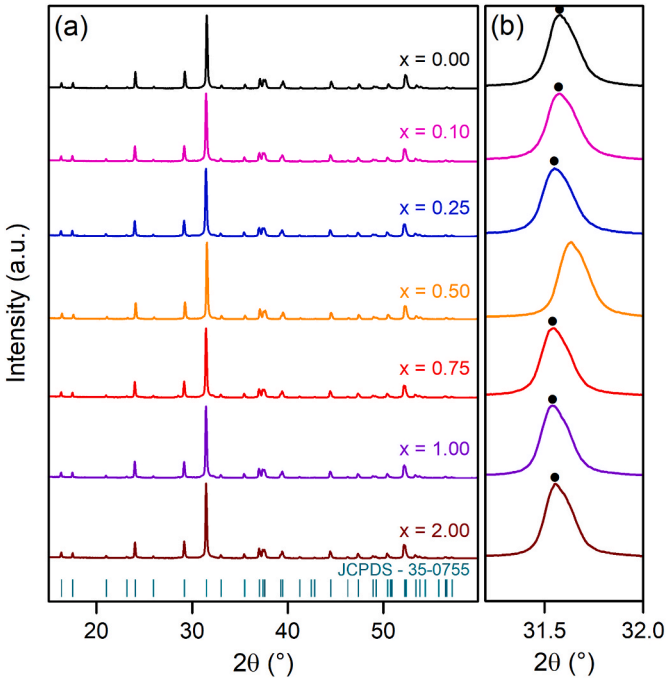

Fig. 1. (a) XRD patterns of phosphor $Ca_2Al_2SiO_7$ doped with *x* mol% Ce (*x* = 0.00, 0.10, 0.25, 0.50, 0.75, 1.00, and 2.00) along with the standard spectrum (shown as vertical green lines). (b) Enlarged view of the XRD spectra in the region 31.2°–32°.

Ce^{3+}-doped $Ca_2Al_2SiO_7$ phosphor. The sharp and strong peaks indicate high crystallinity of the samples. The observed diffraction peaks are related to the tetragonal phase of $Ca_2Al_2SiO_7$ crystal and are consistent with the JCPDS (Joint Committee on Powder Diffraction Standards) card No. 35–0755. No other peaks are observed in the diffractograms besides those corresponding to the $Ca_2Al_2SiO_7$ pattern, which reveals the purity of the crystalline structure of the synthesized materials. Fig. 1b illustrates the shifting of the main peak towards higher 2θ values, the circles representing the peak center. The diffraction peaks were shifted towards higher 2θ values with the increase in Ce -concentration, except for the sample doped with 0.50 mol% Ce.

To study the effect of dopant concentration on the lattice parameters of the host, the XRD data were submitted to Rietveld refinement. The function profile used in the Rietveld refinement was a pseudo-Voigt function, with contributions from Gaussian and Lorentzian functions. The Rietveld refinement of the $Ca_2Al_2SiO_7$ sample is shown in Fig. 2. All observed peaks satisfy the reflection conditions, suggesting the formation of a single phase with no impurities and the observed peaks can be indexed to the corresponding data. The $Ca_2Al_2SiO_7$ phosphors were crystallized in the tetragonal crystal system of space group $P\bar{4}2_1m$ (113). To calculate the average crystalline size and the lattice strain, the Williamson–Hall (W–H) plot method was used [28].

Equation (1) shows the W–H equation:

$$B_{hkl}\cos\theta = \frac{K\lambda}{D} + 4\varepsilon\sin\theta \quad (1)$$

where, B_{hkl} is the width (full-width at half-maximum) of the X-ray diffraction peak in radians and θ is the Bragg angle. $B_{hkl} = B_{obs} - B_{inst}$, where B_{obs} is the experimental peak broadening of a sample pattern, B_{inst} is the instrumental peak broadening computed from a standard pattern of Si. ε is the lattice strain induced in a powder due to crystal imperfections and distortions. K is a numerical factor frequently referred to as the crystalline -shape factor (set to 0.9), and λ is the wavelength of the X-rays (1.541 Å). A plot is drawn with 4 $\sin\theta$ along the x-axis and $B_{hkl}\cos\theta$ along the y-axis. The data points are fitted using a linear model, where the slope represents the lattice strain (ε) and the independent term allows estimation of the average crystalline size (D). Fig. 3 shows the behavior of the average crystalline size of the $Ca_2Al_2SiO_7$ phosphor as a function of dopant concentration. The crystalline sizes are in the micrometer domain, except for the sample with 0.10 mol% Ce dopant, for which it is 561.28 nm, and this is the sample with the highest TL intensity. Fig. 3 presents the lattice strains for all samples; their values are less than 0.14% throughout, confirming high crystallinity in each case. The lattice strain increases consistently for dopant concentrations up to 0.50% above which its value begins to decrease. Refinement parameters, lattice parameters, and cell volumes are presented in Table 1. The goodness-of-fit is less than 5% in all cases, indicating very good consistency between the calculated profile and the experimental data.

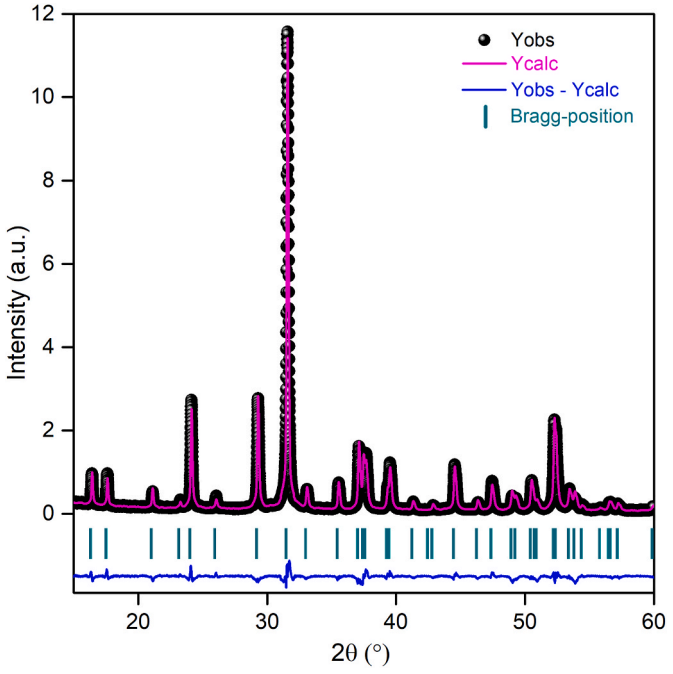

Fig. 2. Rietveld refinement results of the XRD pattern of the Ce-doped $Ca_2Al_2SiO_7$ phosphor, including the experimental (black balls) and calculated (pink line) intensities, as well as differences in intensities between the experimental and calculated data (blue line).

To study the TL properties of the Ce-doped $Ca_2Al_2SiO_7$ samples, one aliquot of each sample was irradiated with γ-rays from a ^{60}Co source with a dose of 20 Gy. Fig. 4 shows the TL curves of all samples. The TL glow curves for the samples show a broad peak centered between 190 °C and 220 °C. Saraswathi et al. [29] observed a similar TL peak for a Dy^{3+} -doped $Ca_2Al_2SiO_7$ sample irradiated with γ-rays of the order of kGy. For our material, the shapes of the glow curves remained the same for all Ce^{3+} concentrations. However, the peak position was seen to shift at higher temperatures with increasing Ce concentration; up to 0.25 mol%, but remained in the same position at 220 °C. The triangles represent the center of each TL peak, and the observed behavior suggests an increase in the peak intensity at 220 °C with decreasing dopant concentration. Furthermore, the TL intensity decays with increasing Ce^{3+} concentration (see the inset in Fig. 4). This behavior of TL sensitivity loss with increasing dopant concentration indicates the destruction of luminescent centers responsible for the emission at the TL peak centered at 220 °C.

Among the glow curves shown in Fig. 4, of greatest interest are those of the samples doped with 0.10 and 0.25 mol% Ce because they reflect a higher sensitivity; the TL intensity of the sample doped with 0.10 mol% Ce is 115 times stronger than that of the undoped sample, highlighting its possible application in dosimetry. On the basis of this observation, the sample doped with 0.10 mol% Ce was selected for further studies.

Fig. 5 shows the TL emission curves of the 0.10 mol% Ce -doped $Ca_2Al_2SiO_7$ sample exposed to γ-rays over the dose range of 1–100 Gy. This sample exhibits a broad glow peak centered at 220 °C along with a shoulder-peak at 350 °C. The intensity of the peak at 220 °C increases linearly with the γ-irradiation dose (see the inset in Fig. 5). This linear behavior of TL intensity with dose for the sample doped with 0.10 mol%

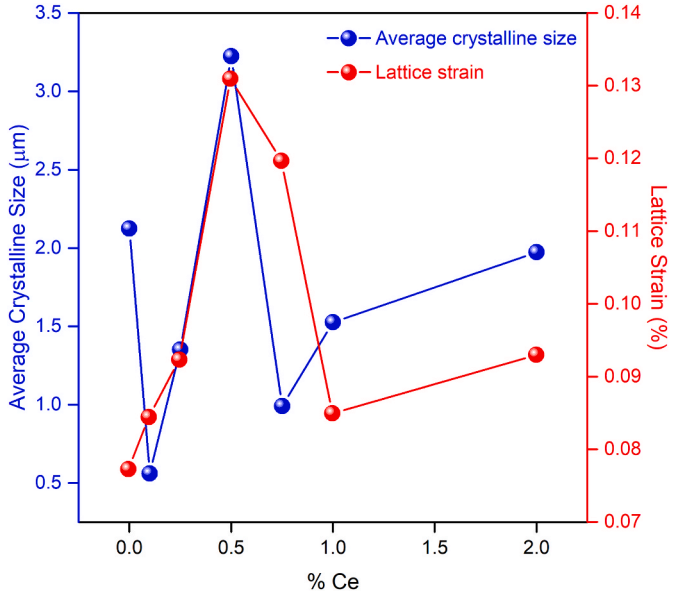

Fig. 3. Average crystalline size and lattice strain in percentage of the $Ca_2Al_2SiO_7$ phosphors as a function of Ce^{3+} concentration.

Table 1
Ce concentration, lattice parameters and volume of $Ca_2Al_2SiO_7$ phosphors from Rietveld refinement are presented. The goodness of fit (GOF) of the refinement are also shown.

Ce concentration mol% Ce	GOF	Lattice parameters			Volume
	χ^2	a and b (Å)	c (Å)	α, β and γ (°)	(Å^3)
0	2.68	7.6744	5.0618	90	298.13
0.10	3.15	7.6747	5.0618	90	298.15
0.25	3.09	7.6729	5.0607	90	297.94
0.50	2.42	7.6759	5.0632	90	298.32
0.75	4.24	7.6756	5.0627	90	298.27
1.00	3.10	7.6745	5.0618	90	298.13
2.00	4.21	7.6759	5.0628	90	298.30

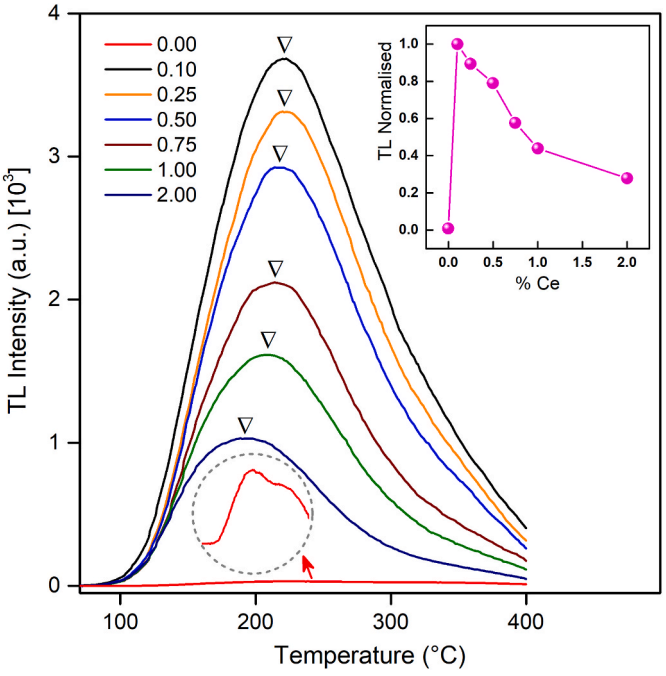

Fig. 4. TL glow curve from irradiated $Ca_2Al_2SiO_7$ phosphor (γ-dose: 20 Gy) with increasing Ce^{3+} concentration. The inset shows the intensity of the 220 °C TL peak with increasing Ce^{3+} concentration in the $Ca_2Al_2SiO_7$ phosphor. The triangles represent the center of each TL peak.

Ce is very useful for dosimetric applications. Further studies on the main TL dosimetric properties of this material are under way.

To evaluate the sensitivity of Ce-doped $Ca_2Al_2SiO_7$, we used an LiF:Mg,Ti (TLD-100) sample (manufactured by Harshaw Bicron) as a comparison standard. Prior to the TL reading, both samples were irradiated with a γ-ray source with a dose of 1 Gy. Fig. 6 shows a comparative plot of the TL intensities between the Ce-doped $Ca_2Al_2SiO_7$ and TLD-100 samples. It can be seen that the Ce-doped $Ca_2Al_2SiO_7$ sample had a TL sensitivity 1.2 times higher than that of TLD-100.

The TL emission spectrum was also recorded for the $Ca_2Al_2SiO_7$ sample doped with 0.10 mol% Ce and is shown in Fig. 7. A band was found in range 300–500 nm, with the peak centered at around 410 nm. This result shows that one recombination center is involved during the TL emission. The TL spectrum features two peaks, one at around 100 °C and the other at 220 °C. The peak at 100 °C is present due to the fact that the TL spectrum was recorded immediately after irradiation.

The TL characterization of the $Ca_2Al_2SiO_7$ phosphor requires knowledge of the kinetic parameters, such as the activation energies of the traps involved in the TL emission, frequency factor (s), and the kinetic order (b) associated with the overlapping glow peaks that give rise

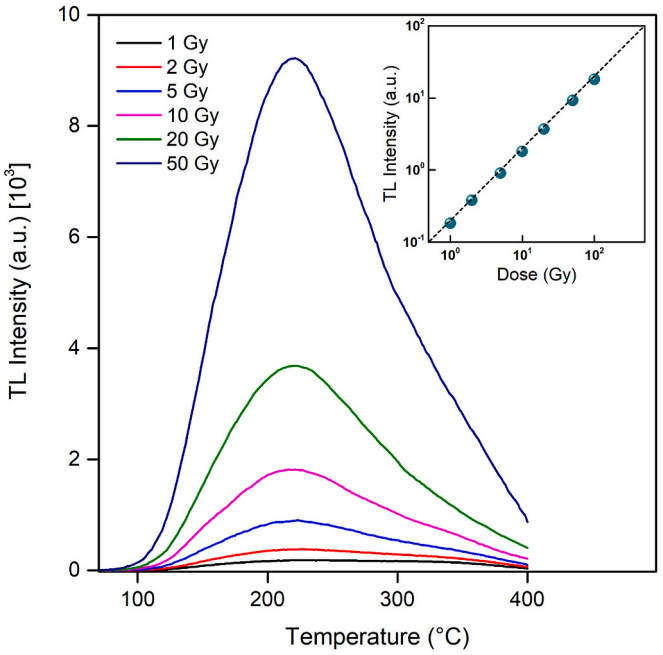

Fig. 5. TL glow curves of Ce-doped $Ca_2Al_2SiO_7$ phosphor irradiated with γ-radiation doses of 1 Gy up to 100 Gy. Inset: intensity variation of the TL peak at 220 °C as a function of γ-radiation dose; the dashed lines (black) indicate linearity.

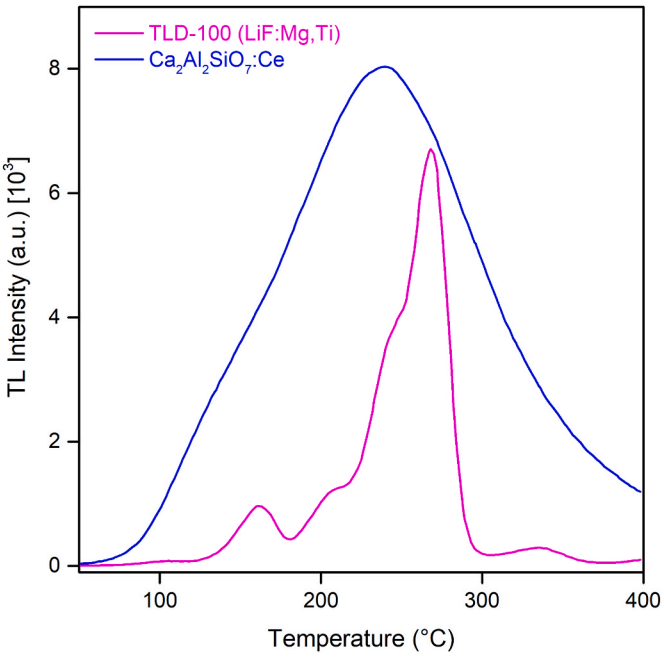

Fig. 6. Comparison of the TL sensitivities of $Ca_2Al_2SiO_7$ and LiF:Mg,Ti (TLD-100) samples after 1 Gy γ-irradiation.

to the broad peak centered at 220 °C. The parameters contained in the complex experimental glow curve of the $Ca_2Al_2SiO_7$ sample can be found by T_m-T_{STOP} [3,30] and deconvolution methods [31,32].

The Tm-T_{STOP} method is used to evaluate the number of peaks, their positions, and their kinetic order [30,33]. A T_m-T_{STOP} graph has a plateau pattern, in which each plateau corresponds to the presence of an individual TL peak [34]. Fig. 8 presents the dependence of T_m on T_{STOP} for the Ce-doped $Ca_2Al_2SiO_7$ sample. In this T_m-T_{STOP} curve, we can delineate two regions corresponding to two TL peaks. The first and

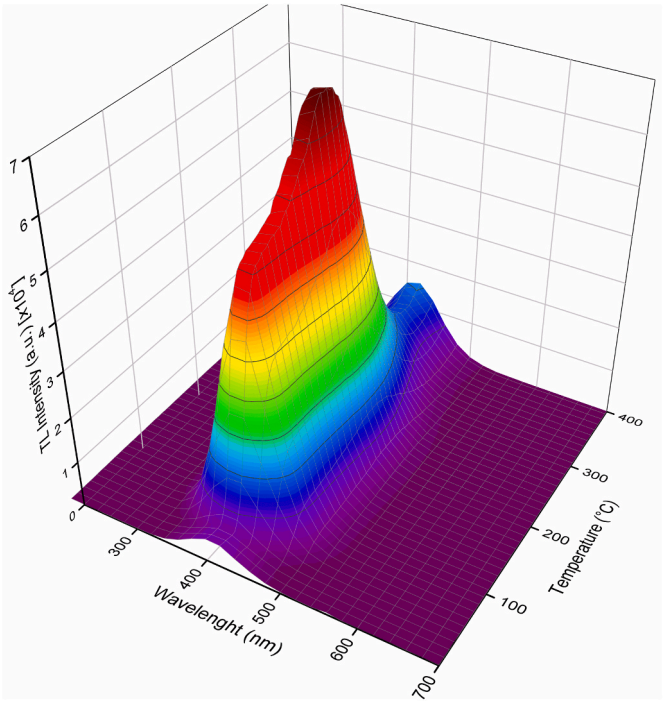

Fig. 7. TL spectra of Ce-doped $Ca_2Al_2SiO_7$ phosphor after β-irradiation.

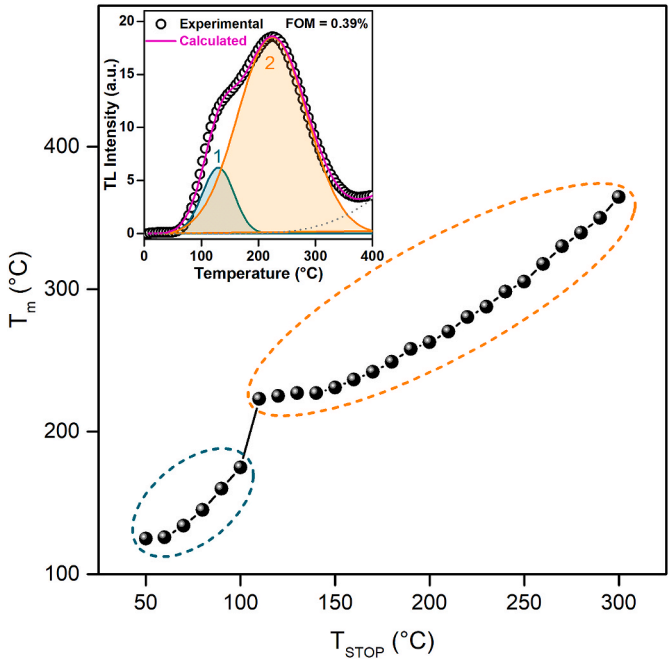

Fig. 8. Dependence of peak maximum temperature (T_m) on preheating temperature (T_{STOP}). The temperature range regions corresponding to the two TL peaks are indicated. The inset shows that a good fit between the experimental glow curve (open circles in black) and the simulated glow curve (full line in pink) can be achieved by assuming the presence of two peaks.

second regions corresponding to the first and second TL peaks, respectively, show a gradual growth in T_m. This behavior of the T_m-T_{STOP} curve, together with the result in Fig. 5, indicates that each TL peak is probably a superposition of more than one TL peak with first-order kinetics. Moreover, it is known from the literature that such behavior of the T_m-T_{STOP} curve may be caused by the presence of several overlapping TL peaks that obey a certain energy distribution of the continuous traps [30]. From this preliminary analysis, we assume that both TL peaks are due to a distribution of continuous traps with first-order kinetics. After preliminary analysis to establish that each TL peak was indeed constituted by a continuous distribution of energy traps, deconvolution of the glow curve was performed using a linear combination of two functions related to the FOK (first-order kinetics) approach, with continuous trap contributions conforming to a Gaussian distribution. The inset in Fig. 8 shows the deconvolution of the glow curve into two TL peaks using first-order kinetic trap distributions for each TL peak in the region between 50 and 350 °C. The above analysis shows that the broad TL glow curve of the $Ca_2Al_2SiO_7$ phosphor sample is composed of two TL peaks centered at 120 and 220 °C. A successful deconvolution process is guaranteed by minimizing the figure of merit (FOM) [35] value. As can be seen from the low FOM value of = 0.39%, the curve deconvolution analysis process was very accurate. The kinetic parameters obtained by the deconvolution method for each peak are shown in Table 2.

Fig. 9 shows the continuous-wave OSL (CW-OSL) curves of $Ca_2Al_2SiO_7$ phosphor with different Ce concentrations (0.10, 0.25, 0.50, 1.00 and 2.00 mol%). For OSL measurements, all samples of equal mass in powder form were first irradiated in situ with a $^{90}Sr/^{90}Y$ β-source with a dose of 4.01 Gy. OSL intensities were determined using the first point of the OSL signal. The samples doped with 0.10 and 0.25 mol% Ce were found to be more sensitive, as shown in the inset of Fig. 9. Therefore, the subsequent OSL study was centered on this material. Meanwhile, the pure $Ca_2Al_2SiO_7$ material (undoped with Ce) showed negligible OSL signals, implying that Ce doping introduces the defects or luminescent centers necessary for its OSL emission. Unlike TL, the OSL response shows an increase with increasing Ce dopant concentration up to 0.25 mol%. For concentrations above this value, the OSL response gradually decreases.

Despite showing a lower sensitivity in its OSL response compared to its TL response, a study of the OSL intensity behavior as a function of dose was performed for the 0.10 mol% doped $Ca_2Al_2SiO_7$ material. For this purpose, aliquots of approximately the same powder mass were irradiated with β-doses in the range from 0.41 to 16.2 Gy. The OSL decay curves of the Ce-doped $Ca_2Al_2SiO_7$ phosphor for various absorbed doses are shown in Fig. 10. The OSL intensity is seen to increase with increasing β-dose. The behavior of the OSL signal with respect to dose is seen to be slightly linear in the applied dose range (see the inset in Fig. 10). This result implies that the synthesized material may have potential application in dosimetry, but a detailed study is necessary to confirm its applicability in dosimetry by analysis of its dosimetric characteristics.

The room-temperature EPR spectra of γ-irradiated Ce-doped $Ca_2Al_2SiO_7$ phosphor at different γ-doses from 10 Gy to 500 Gy are shown in Fig. 11. The inset shows the variation in the intensity of center I with γ-dose. The spectrum consists four dominant lines that result from interaction of the electron spin with a spin 3/2 nucleus. Thermal annealing experiments reveal an overlap of two groups of four lines in the spectrum, which result from two distinct defect centers. These two centers are labeled in Fig. 11. EPR spectral simulations indicate the presence of an additional single line which is also labeled in Fig. 11 as center III. The center III line is overlapped by the relatively high-intensity center I and II lines. Center I, with four-line hyperfine splitting, is characterized by a g-value of 2.0090, and the hyperfine splitting is estimated to be 10.5 G.

Table 2
Details of maximum temperature (T_M), activation energy (E), distribution width (σ), frequency factors (s) of TL peaks of $Ca_2Al_2SiO_7$ phosphor obtained by deconvolution method. FOM = 039%.

Peak	T_M (°C)	E (eV)	σ (eV)	s (s^{-1})
1	127	0.937	0.055	$1.72 \cdot 10^{11}$
2	225	1.106	0.13	$3.19 \cdot 10^{10}$

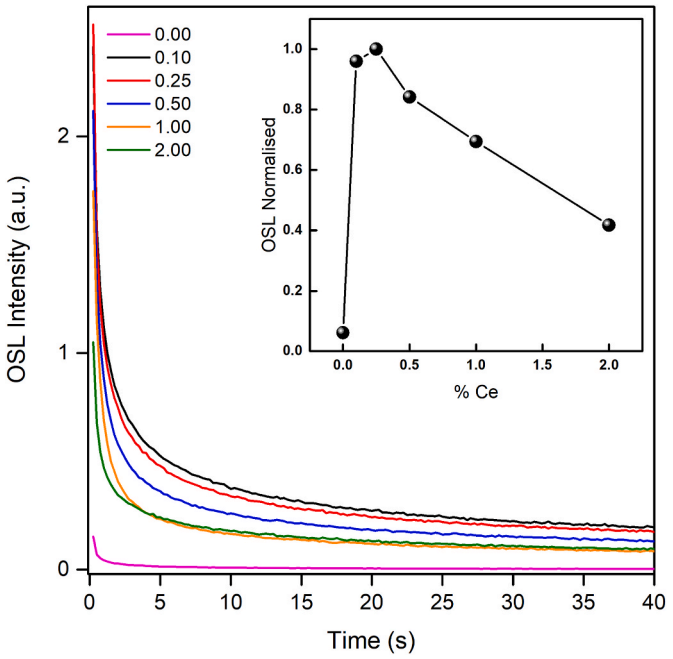

Fig. 9. OSL decay curve of $Ca_2Al_2SiO_7$ phosphor (after irradiating to 4.05 Gy and stimulated with blue light) with different Ce^{3+} concentrations. Inset: Ce^{3+}-concentration dependence of OSL intensity.

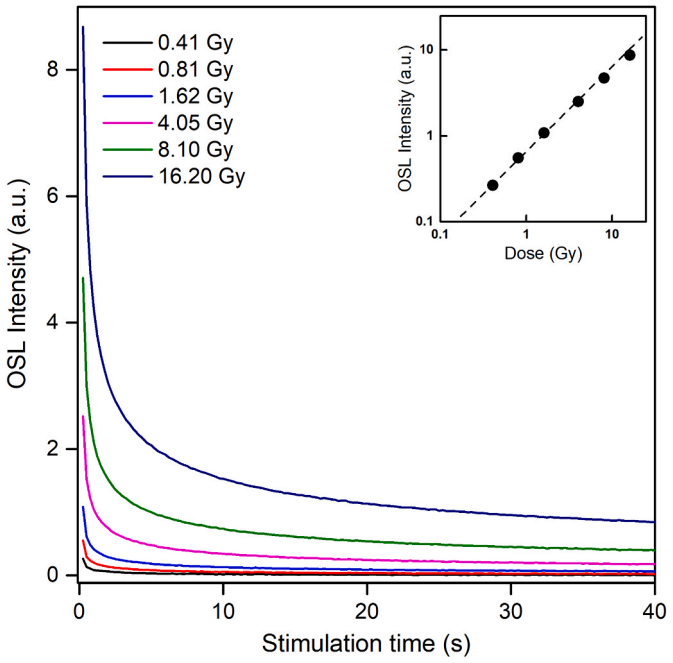

Fig. 10. OSL decay curves (under blue-light stimulation) of Ce-doped $Ca_2Al_2SiO_7$ phosphor in powder irradiated with different β-radiation doses of 0.41 Gy up to 16.2 Gy. Inset: OSL intensity behavior as a function of β-radiation dose, the dashed lines (black) indicate linearity.

$Ca_2Al_2SiO_7$ is a typical melilite compound crystallizing in the tetragonal crystal system with space group $P\bar{4}2_1m$. The cations (Ca^{2+}, Al^{3+}, and Si^{4+}) are localized at three types of site. The Ca^{2+} ion occupies an eightfold coordinated site known as a Thomson cube (TC) site, and a regular tetrahedral site (T_1) is fully occupied by half of the Al^{3+} ions [36,37]. Further, Si^{4+} and the other half of the Al^{3+} ions are statistically distributed over a very distorted tetrahedral site (T_2). Thomson cubes

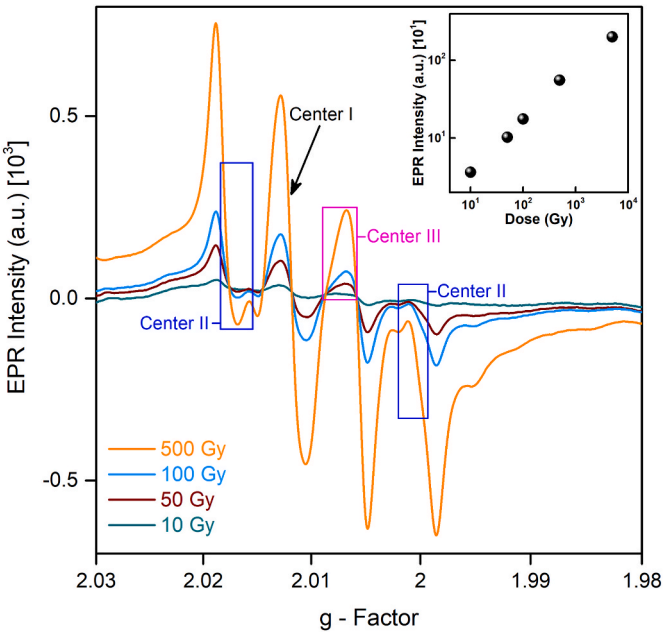

Fig. 11. Room temperature EPR spectra of irradiated Ce-doped $Ca_2Al_2SiO_7$ phosphor for different γ-doses. Line labeled as center I is due to an O^- ion. Center II line is also assigned to an O^- ion and center III is attributed as an F^+ center. The inset shows the intensity variation of the center I line with γ-dose.

and tetrahedra are alternately stacked along the *z*-axis and the sheets are linked by Ca^{2+} ions.

The Ca^{2+} ion has an ionic radius of 1.12 Å in eightfold coordination [38]. The ionic radius of Al^{3+} ion in a fourfold coordination is 0.39 Å. The Si^{4+} ion, which resides in a tetrahedral coordination, has an ionic radius of 0.26 Å. The Ce^{3+} ion has an ionic radius of 1.14 Å in an eightfold coordination. As four-coordinated Al^{3+} and Si^{4+} are relatively small compared to a Ce^{3+} ion, the dopant Ce^{3+} tends to preferentially occupy the Ca^{2+} sites (see Fig. 12).

In a perfect lattice of $Ca_2Al_2SiO_7$, Ca^{2+}, Al^{3+}, and Si^{4+} would be expected to be located in their respective sites. However, anti-site cation-exchange is likely to occur in $Ca_2Al_2SiO_7$, whereby Si^{4+} ions partially replace Ca or Al sites. These replacements, termed cation-exchange disorder, give rise to point defects in crystals, whereby cations exchange positions. Kuklja [39] has predicted the occurrence of such defects based on theoretical calculations. This prediction is supported by X-ray diffraction [40] and X-ray absorption fine structure studies by Dong et al. [41]. The effects of such disorder on luminescence properties have been demonstrated in a study of Cr^{3+} ion in an AB_2O_4 spinel host lattice [42].

Anti-site formation due to interchange of ions gives rise to several trapping sites for electron and holes upon irradiation. Therefore, several defect centers are likely to be formed in a system such as $Ca_2Al_2SiO_7$, the most probable of which are an F^+ center (an electron trapped at an anion vacancy) and an O^- ion (a positive hole localized on an O^- ion adjacent to a cation vacancy). Trapping of an electron at an anion vacancy can be induced by γ-irradiation, leading to the formation of an F^+ center. Studies by Yuan et al. [43] have shown that anion vacancies can be formed more easily in a lattice with cation disorder as compared to a perfect lattice. On the other hand, cation vacancies can trap holes to form O^- ions [44].

The oxygen p-orbital in an O^- ion contains the unpaired spin and a cation vacancy located adjacent to the O^- ion stabilizes the hole through electrostatic attraction. A positive *g*-shift results from a hole trapped in an oxygen p_z orbital. Center I is characterized by a *g*-value of 2.0089 and displays a positive *g*-shift. As this *g*-shift is rather large, center I is tentatively identified as an O^- ion formed by hole trapping at an O^{2-} ion

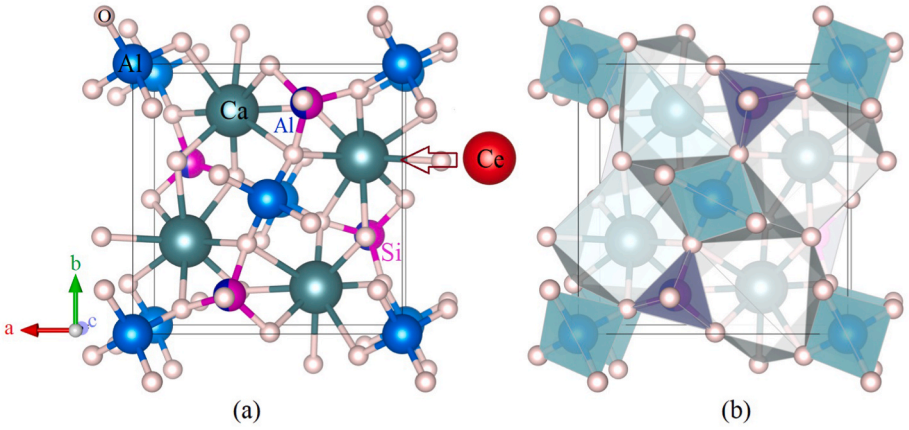

Fig. 12. (a) The tetragonal crystal structure of $Ca_2Al_2SiO_7$ projected on to the (001) plane, showing the positions of the Ca, Al, Si, and O atoms. (b) A view of the environments of the Ca, Al, Si, and O atoms. A Ce^{3+} ion substitutes the Ca^{2+} ion and an F^+ center forms at an anion vacancy.

adjacent to a cation vacancy. Center I displays an isotropic *g*-value. However, O^- ions are generally characterized by an axial *g*-tensor, with the perpendicular component greater than the free-spin value (g_e = 2.0023) and the parallel component close to g_e [45]. There are also cases in which the O^- ion exhibits a rhombic *g*-tensor. In anatase nanoparticles, Misra et al. [46] observed a rhombic *g*-tensor with principal values of $g_x = 2.0$, $g_y = 2.01$ and $g_z = 2.03$. On the other hand, there are studies in which O^- displays an isotropic *g*-value. An example concerns $MgAl_2O_4$, whereby X-ray irradiation resulted in a center with a *g*-value of 2.011 and an optical absorption band at 3.4 eV [47]. Ibarra et al. [47] concluded, based on optical absorption studies, that the center in $MgAl_2O_4$ is a hole-trapped cation vacancy (V-type center). Indeed, the assignment of center I as an O^- ion in the present study is mainly based on the observations of Ibarra et al. [47].

The stability of center I was measured by a pulse-thermal annealing method. After heating the sample to a given temperature, it was maintained at that temperature for 3 min. It was then cooled to room temperature for EPR measurements. Fig. 13 shows the thermal annealing behavior of center I. It is observed that this center becomes unstable at about 120 °C and decays in the temperature region 120–280 °C. This decay indicates that center I is related to the TL peak at 220 °C.

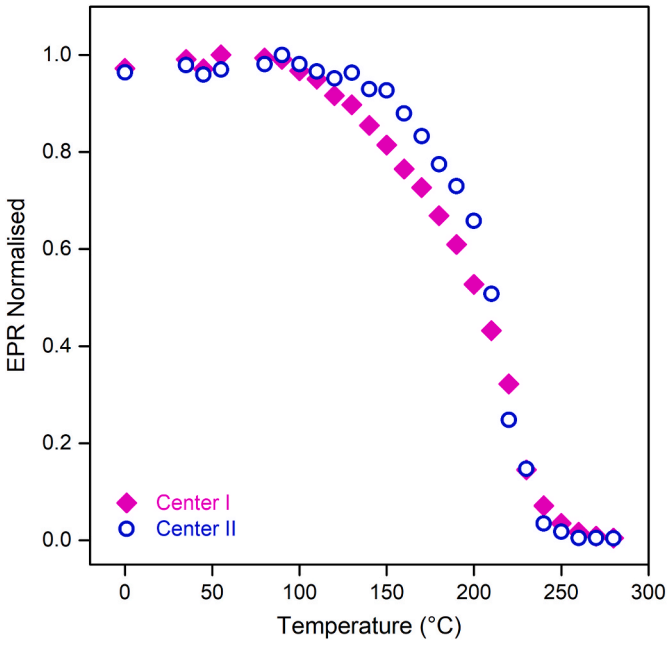

Fig. 13. Thermal annealing behavior of center I and center II in Ce -doped $Ca_2Al_2SiO_7$ phosphor.

The EPR lines labeled as center II in Fig. 11 are due to a distinct center with an isotropic *g*-factor of 2.0073. This center displays hyperfine lines due to an interaction with a spin I = 3/2 nucleus, and the hyperfine splitting is 7.8 Gauss. Based on the reasons mentioned above for the assignment of center I, center II is also ascribed to an O^- ion. The four lines may have arisen due to an interaction with a ^{23}Na nucleus present in the system as an impurity ion. The thermal annealing behavior of this center is shown in Fig. 13. The intensity of the EPR lines starts to reduce at about 170 °C and the center decays in the temperature range 170–280 °C. Center II also appears to correlate with the TL peak at 220 °C.

A careful examination of the EPR spectrum around magnetic field 3375 Gauss (Fig. 11) indicates an EPR line that is overlapped by the dominant lines of centers I and II. An EPR spectral simulation has been carried out to unravel the presence of this line. The observed spectrum for Ce-doped $Ca_2Al_2SiO_7$ was simulated using the parameters derived from the experimental spectrum. The center I spectrum was simulated using parameters of $g = 2.0090$ and A = 10.5 Gauss, and the linewidth of the individual hyperfine line was taken to be 2.6 Gauss. For center II, the parameters $g = 2.0073$ and A = 7.8 Gauss, along with a linewidth of 2.9 Gauss, were considered for each individual line of the four-line spectrum. These simulated spectra are shown in Fig. 14. The correlation between the simulated and experimental spectra appears to be reasonably good. Center III parameters derived from this simulation are g = 2.0076 with a linewidth of 2.8 Gauss.

It was mentioned earlier that one of the probable centers that can form in Ce-doped $Ca_2Al_2SiO_7$ is the F^+ center (an electron trapped at an anion vacancy) as a result of the presence of cation disorder. An F center was first observed in neutron-irradiated LiF [48]. A very broad line (linewidth ca. 100 Gauss), unusual for a defect center, was observed with a *g*-value of 2.008. The linewidth of the F center here, however, is quite small. In MgO [49], the center displays its inherent linewidth of about 1 Gauss. The ions present in a lattice, the natural abundance, the magnetic moments of the nuclei, and the degree of delocalization of the unpaired spins determine the experimentally observed linewidth.

The extent of delocalization of the unpaired electron depends on the host lattice. For example, in alkali metal halides, relatively large linewidths are observed as the unpaired electron interacts with several alkali metal and halide ions from successive neighboring shells. In LiCl, the observed linewidth is 58 Gauss [50], whereas in KCl, it is about 20 Gauss [50]. In systems such as BaO [51] and HgI_2–2HgO [52], the observed linewidths are 35 Gauss and 10 Gauss, respectively. Electrons trapped at anion vacancies have also been observed in oxide systems. It is observed that F^+ centers display *g*-values close to the free-electron

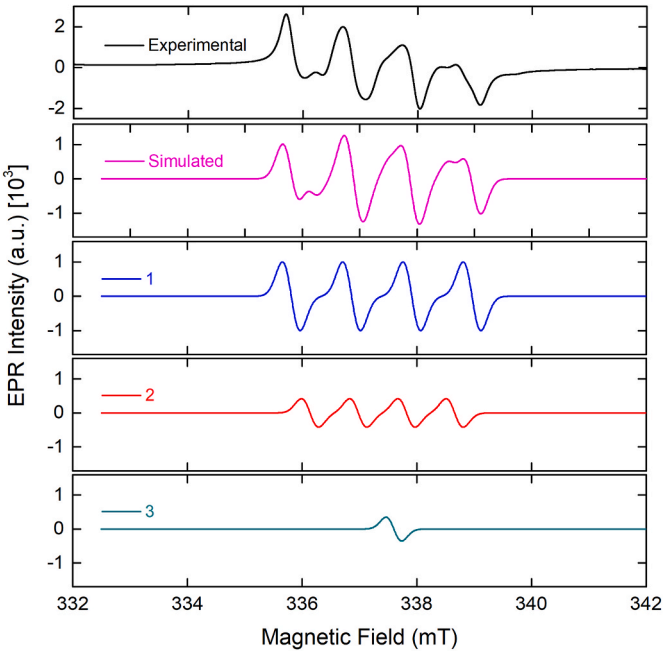

Fig. 14. Simulated and experimental EPR spectra of Ce -doped $Ca_2Al_2SiO_7$ phosphor. Spectra marked 1, 2, and 3 are the simulated spectra of centers I, II, and III, respectively. The combined simulated spectrum of the three centers is labeled as "simulated".

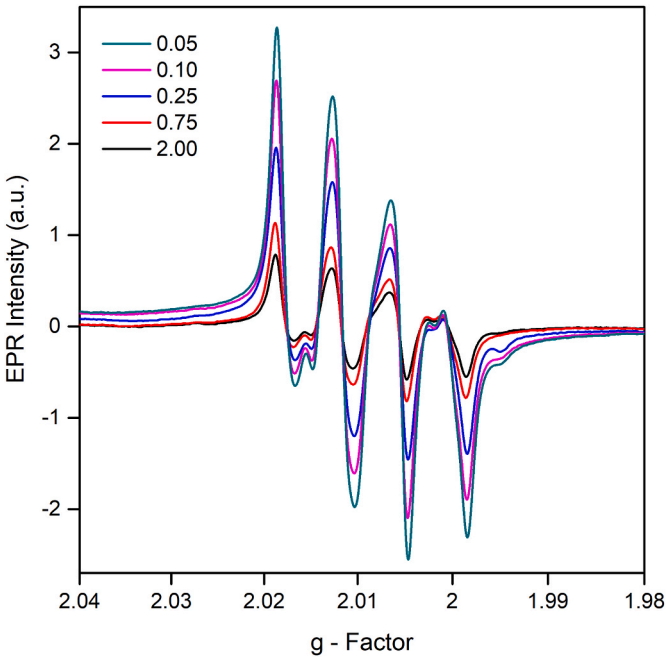

Fig. 15. EPR spectrum of irradiated Ce-doped $Ca_2Al_2SiO_7$ phosphor (γ-dose: 5 kGy) with increasing Ce^{3+} -dopant ion.

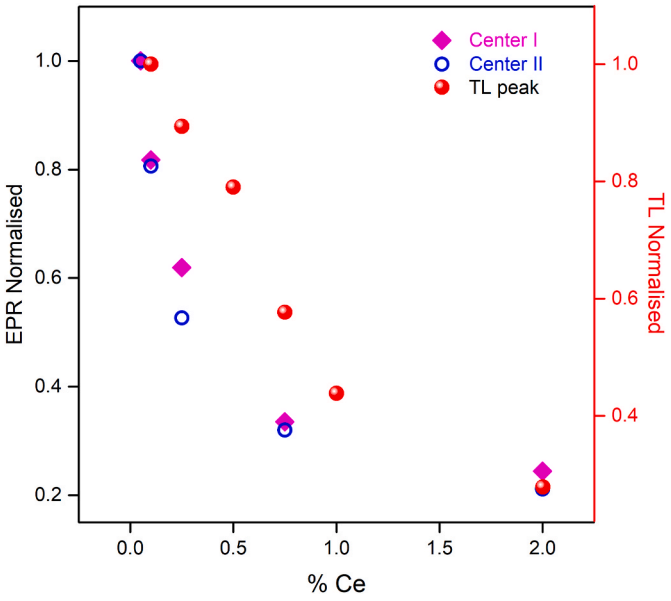

Fig. 16. Effect of increasing Ce^{3+} concentration on the EPR signal intensity of centers I and II and the intensity of the 220 °C TL peak for the $Ca_2Al_2SiO_7$ phosphor.

value (2.0023) and a *g*-shift that may be positive or negative. Center III observed in the Ce-doped $Ca_2Al_2SiO_7$ phosphor is characterized by a relatively small *g*-shift and the linewidth is not large. Based on these observations and consideration of the likely defects that may be formed in a system such as Ce-doped $Ca_2Al_2SiO_7$, center III is tentatively assigned as an F^+ center. It proved difficult to follow the center III EPR line during thermal annealing experiments as the line was barely seen. Thus, it was not possible to associate this center with the observed TL peaks.

Studies were carried out to observe the effect of increasing Ce^{3+} ion concentration on the EPR spectrum as well as the TL glow curve. The results of these experiments are shown in Fig. 15 and Fig. 4. It can be seen that the intensities of the EPR signals associated with centers I and II decreased with increasing Ce^{3+} ion concentration in the lattice (see Fig. 15). The Ce^{3+} ion dopant was observed to have the same effect on the 220 °C TL glow peak, that is, decreasing TL intensity with increasing dopant concentration (inset of Fig. 4). The measured EPR and TL intensities are displayed in Fig. 16. The results are in accordance with the hypothesis that centers I and II correlate with the 220 °C TL peak, such that a decrease in TL intensity would be expected with decreasing center I and II concentrations in the lattice. As the trivalent Ce^{3+} ion concentration is increased in $Ca_2Al_2SiO_7$, there will be excess positive charge in the lattice. Charge neutrality requirements necessitate the creation of cation vacancies or an increase in the amount of negative ions in the lattice. O^- ions (centers I and II) are formed by hole capture by O^{2-} ions and their formation reduces the negative charge. This formation is restrained by excessive positive charge in the lattice due to a high concentration of Ce^{3+} ions. It is speculated that this results in a reduction in the amount of O^- ions with increasing Ce^{3+} ion in $Ca_2Al_2SiO_7$ (see Fig. 16).

4. Conclusions

The XRD results indicate that in all of the samples, the Ce dopant concentration does not change the tetragonal phase of the $Ca_2Al_2SiO_7$. The average crystalline sizes are in the micrometer domain and vary with the concentration of the Ce dopant. The minimum value is 561.28 nm for 0.10 mol% Ce, which corresponds to the sample with the highest TL intensity. In all samples, the lattice strains are less than 5%, which implies that they have a high proportion of crystallinity. TL studies revealed a broad peak centered at 220 °C with a TL emission band at 410 nm. The activation energy (*E*), frequency factor (*s*), and kinetic order have been estimated using T_m-T_{STOP} and deconvolution methods. From detailed TL and OSL studies of the Ce-doped $Ca_2Al_2SiO_7$, the sample doped with 0.10 mol% Ce proved to be most sensitive. Specifically, its TL and OSL responses are approximately 115 and 16.25 times higher, respectively, than those of undoped $Ca_2Al_2SiO_7$. The TL and OSL intensities of the synthesized $Ca_2Al_2SiO_7$ samples increased with increasing radiation dose. The TL and OSL dose-response curves are

linear in the dose ranges of 1–50 Gy and 0.41–16.2 Gy, respectively, suggesting that this phosphor is suitable for radiation dosimetry applications using the TL and OSL techniques. Three defect centers have been identified in γ-irradiated Ce-doped $Ca_2Al_2SiO_7$ phosphor. These centers are tentatively assigned to O^- ions and an F^+ center. The two O^- ions correlate with the dominant 220 °C TL peak. As there is considerable overlap, no specific TL role could be assigned to the F^+ center.

CRediT authorship contribution statement

Nilo F. Cano: Writing – original draft, Supervision, Funding acquisition, Conceptualization, Project administration, Writing – review & editing. **Amador J. Gonsalez-Vasquez**: Investigation, Methodology. **T. K. Gundu Rao**: Writing – original draft, Validation, Investigation, Visualization. **Klinton V. Turpo-Huahuasoncco**: Investigation, Software. **Edwar A. Canaza-Mamani**: Investigation. **Alejandro H. Lopez-Gonzales**: Investigation, Software, Writing – review & editing. **Henry S. Javier-Ccallata**: Investigation, Methodology. **Jorge S. Ayala-Arenas**: Project administration, Investigaction. **René R. Rocca**: Investigation, Methodology. **Noemi B. Silva-Carrera**: Investigation. **Jose F.D. Chubaci**: Investigation. **Shigueo Watanabe**: Resources, Investigation.

Declaration of competing interest

The authors declare that they have no known competing financial interests or personal relationships that could have appeared to influence the work reported in this paper.

Data availability

The data that has been used is confidential.

Acknowledgements

The authors would like to express thanks to Ms. E. Somessari from the Institute for Energy and Nuclear Researches (IPEN), Brazil, for kindly carrying out the γ-irradiation of the samples. This work was partially supported by CONCYTEC-FONDECYT, Peru, in the framework of the call E038-01 (Process number 037–2019).

References

[1] L. Boetter-Jensen, S.W.S. McKeever, A.G. Wintle, Optically Stimulated Luminescence Dosimetry, Elsevier Science, 2003.
[2] E.G. Yukihara, S.W.S. McKeever, Optically Stimulated Luminescence: Fundamentals and Applications, John Wiley & Sons, Ltd., 2011.
[3] S.W.S. McKeever, Thermoluminescence of Solids, Cambridge University Press, London, 1985.
[4] A. Marfunin, Spectroscopy: Luminescence and Radiation Centers in Minerals, Springer, Berlin, 1979.
[5] B. Simondi-Teisseire, B. Viana, D. Vivien, A.M. Lejus, Optical investigation of Er: $Ca_2Al_2SiO_7$ and Yb:$Ca_2Al_2SiO_7$ for lasers applications in the near infrared, Phys. Status Solidi 155 (1996) 249–262, https://doi.org/10.1002/pssa.2211550125.
[6] A.M. Lejus, N. Pelletier-Allard, R. Pelletier, Site selective spectroscopy of Nd ions in gehlenite ($Ca_2Al_2SiO_7$), a new laser material, Opt. Mater. 6 (1996) 129–137, https://doi.org/10.1016/0925-3467(96)00041-9.
[7] J. Cai, H. Pan, Y. Wang, Luminescence properties of red-emitting $Ca_2Al_2SiO_7$:Eu^{3+} nanoparticles prepared by sol-gel method, Rare Met. 30 (2011) 374–380, https://doi.org/10.1007/s12598-011-0399-x.
[8] N.M. Son, D.T. Tien, D.T. Tien, P.N. Luyen, N.V. Tam, N.V. Hung, L.T. Cang, Spectroscopic characteristics of $Ca_2Al_2SiO_7$: RE^{3+} phosphors, Int. J. Eng. Tech. Res. 8 (2019) 1509–1512.
[9] H. Jiao, Y. Wang, $Ca_2Al_2SiO_7$: Ce^{3+}, Tb^{3+}: a white-light phosphor suitable for white-light-emitting diodes, J. Electrochem. Soc. 156 (2009) J117–J120, https://doi.org/10.1149/1.3097191.
[10] X.J. Wang, D. Jia, W.M. Yen, Mn^{2+} activated green, yellow, and red long persistent phosphors, J. Lumin. 102–103 (2003) 34–37, https://doi.org/10.1016/S0022-2313(02)00541-0.
[11] M. Yamaga, Y. Oshumi, T. Nakayama, N. Kashiwagura, N. Kodama, T.P.J. Han, Long-lasting phosphorescence in Ce-doped oxides, J. Mater. Sci. Mater. Electron. 20 (2009) 471–475, https://doi.org/10.1007/s10854-008-9683-4.
[12] H. Wu, Y. Hu, G. Ju, L. Chen, X. Wang, Z. Yang, Photoluminescence and thermoluminescence of Ce^{3+} and Eu^{2+} in $Ca_2Al_2SiO_7$ matrix, J. Lumin. 131 (2011) 2441–2445, https://doi.org/10.1016/j.jlumin.2011.06.024.
[13] P. Yang, X. Yu, H. Yu, T. Jiang, X. Xu, Z. Yang, D. Zhou, Z. Song, Y. Yang, Z. Zhao, J. Qiu, , $Ca_2Al_2SiO_7$:Bi^{3+}, Tb3+ Eu, A potential single-phased tunable-color-emitting phosphor, J. Lumin. 135 (2013) 206–210, https://doi.org/10.1016/j.jlumin.2012.10.015.
[14] X.H. Chuai, H.J. Zhang, F.Sh Li, K.Ch Chou, The luminescence of Eu^{3+} ion in $Ca_2Al_2SiO_7$, Opt. Mater. 25 (2004) 301–305, https://doi.org/10.1016/j.optmat.2003.08.008.
[15] G. Tiwari, N. Brahme, R. Sharma, D.P. Bisen, S.K. Sao, I.P. Sahu, $Ca_2Al_2SiO_7$:Ce^{3+} phosphors for mechanoluminescence dosimetry, Luminescence 31 (2016) 1479–1487, https://doi.org/10.1002/bio.3133.
[16] G. Tiwari, N. Brahme, R. Sharma, D.P. Bisen, S.K. Sao, S.J. Dhoble, A study on the luminescence properties of gamma-ray- irradiated white light emitting $Ca_2Al_2SiO_7$: Dy^{3+} phosphors fabricated using a combustion-assisted method, RSC Adv. 6 (2016) 49317–49320, https://doi.org/10.1039/C6RA04913C.
[17] S. Sharma, N. Brahme, D.P. Bisen, P. Dewangan, Cool white light emission from Dy^{3+} activated alkaline alumino silicate phosphors, Opt Express 26 (2018) 29495–29508, https://doi.org/10.1364/OE.26.029495.
[18] S. Sharma, N. Brahme, D.P. Bisen, P. Dewangan, S. Tigga, G. Tiwari, A. Khare, Study on photoluminescence and thermoluminescence properties of UV-irradiated $CaSrAl_2SiO_7$:Ce^{3+} phosphors, J. Mater. Sci. Mater. Electron. 29 (2018) 1412–1419, https://doi.org/10.1007/s10854-017-8048-2.
[19] M. Hagiwara, H. Noguchi, T. Hoshina, H. Takeda, S. Fujihara, N. Kodama, T. Tsurumi, Growth and characterization of $Ca_2Al_2SiO_7$ piezoelectric single crystals for high-temperature sensor applications, Jpn. J. Appl. Phys. 52 (2013) 1–5, https://doi.org/10.7567/JJAP.52.09KD03.
[20] W. Wei, Y.P. Qi, S.Y. Nikonov, L. Niu, R.L.W. Messer, J. Mao, C.M. Primus, D. H. Pashley, F.R. Tay, Effects of an experimental calcium aluminosilicate cement on the viability of murine odontoblast-like cells, J. endodontics 38 (2012) 936–942, https://doi.org/10.1016/j.joen.2012.03.020.
[21] N. Kodama, Y. Tani, M. Yamaga, Optical properties of long-lasting phosphorescent crystals Ce^{3+}-doped $Ca_2Al_2SiO_7$ and $CaYAl_3O_7$, J. Lumin. 87–89 (2000) 1076–1078, https://doi.org/10.1016/S0022-2313(99)00543-8.
[22] E.A. Canaza-Mamani, N.F. Cano, J. Mosqueira-Yauri, T.K. Gundu Rao, S.C. Aynaya-Cahui, A.J. Gonsalez-Vasquez, M.B. Gomes, J.F.D. Chubaci, S. Watanabe, J. S. Ayala-Arenas, TL and EPR characteristics of $SrAl_2O_4$ phosphor prepared by solid-state reaction method, J. Lumin. 245 (2022), 118585, https://doi.org/10.1016/j.jlumin.2021.118585.
[23] S.C. Aynaya-Cahui, N.F. Cano, A.H. Lopez-Gonzales, T.K. Gundu Rao, M.B. Gomes, R.R. Rocca, J.F.D. Chubaci, S. Watanabe, J.S. Ayala-Arenas, Thermoluminescence and electron paramagnetic resonance correlation studies in lithium silicate phosphor, Solid State Sci. 123 (2021), 106777, https://doi.org/10.1016/j.solidstatesciences.2021.106777.
[24] N.F. Cano, T.K. Gundu Rao, B.N. Silva-Carrera, S.P.S. Cruz, H.S. Javier-Ccallata, Y. A. Bedoya-Barriga, J.S. Ayala-Arenas, S. Watanabe, Elucidation of the centers responsible for the TL peaks in the anhydride crystal, J. Lumin. 221 (2020), 117082, https://doi.org/10.1016/j.jlumin.2020.117082.
[25] N.F. Cano, T.K. Gundu Rao, C.D. Gonzales-Lorenzo, J.S. Ayala-Arenas, H.S. Javier-Ccallata, S. Watanabe, Thermoluminescence and defect centers in synthetic diopside, J. Lumin. 211 (2019) 314–319, https://doi.org/10.1016/j.jlumin.2019.03.038.
[26] N.F. Cano, T.K. Gundu Rao, J.S. Ayala-Arenas, C.D. Gonzales-Lorenzo, L. M. Oliveira, S. Watanabe, TL in green tourmaline: study of the centers responsible for the TL emission by EPR analysis, J. Lumin. 205 (2018) 324–328, https://doi.org/10.1016/j.jlumin.2018.09.034, 2018.
[27] J.M. Yauri, N.F. Cano, S. Watanabe, Tl, EPR and optical absorption in natural grossular crystal, J. Lumin. 128 (2008) 1731–1737, https://doi.org/10.1016/j.jlumin.2008.03.021.
[28] W.H. Hall, X-ray line broadening in metals, Proc. Phys. Soc. 62 (1949) 741, https://doi.org/10.1088/0370-1298/62/11/110.
[29] A.V. Saraswathi, N.S. Prabhu, K. Naregundi, M.I. Sayyed, M.S. Murari, A. H. Almuqrin, S.D. Kamatha, Thermoluminescence investigations of $Ca_2Al_2SiO_7$: Dy^{3+} phosphor for gamma dosimetry applications, Mater. Chem. Phys. 281 (2022), 125872, https://doi.org/10.1016/j.matchemphys.2022.125872G.
[30] S.W.S. McKeever, On the analysis of complex thermoluminescence glow-curves: resolution into individual peaks, Phys. Status Solidi 62 (1980) 331–340, https://doi.org/10.1002/pssa.2210620139.
[31] G. Kitis, J.M. Gómez-Ros, W.N. Tuyn, Thermoluminescence glow-curve deconvolution functions for first, second and general orders of kinetics, J. Phys. D Appl. Phys. 31 (1998) 2636–2641, https://doi.org/10.1088/0022-3727/31/19/037.
[32] J.F. Benavente, J.M. Gómez-Ros, A.M. Romero, Thermoluminescence glow curve deconvolution for discrete and continuous trap distributions, Appl. Radiat. Isot. 153 (2019), 108843, https://doi.org/10.1016/j.apradiso.2019.108843.
[33] C. Furetta, Handbook of Thermoluminescence, World Scientific -Physics Department Rome University "La Sapienza, Roma, 2003.
[34] W. Gieszczyk, D. Kulig, P. Bilski, B. Marczewska, M. Kłosowski, Analysis of TL and OSL kinetics in lithium magnesium phosphate crystals, Radiat. Meas. 106 (2017) 100–106, https://doi.org/10.1016/j.radmeas.2017.04.008.
[35] H.G. Balian, N.W. Eddy, Figure of merit (FOM), an improved criterion over the normalised chi-squared test for assessing goodness-of-fit of gamma ray spectra peaks, Nucl. Instrum. Methods 145 (1977) 389–395, https://doi.org/10.1016/0029-554X(77)90437-2.

[36] A.M. Lejus, A. Kahn-Harari, J.M. Benitez, B. Viana, Crystal growth, characterization and structure refinement of neodymium^{3+} doped gehlenite, a new laser material [$Ca_2Al_2SiO_7$], Mater. Res. Bull. 29 (1994) 725–734, https://doi.org/10.1016/0025-5408(94)90197-X.

[37] P. Florian, E. Veron, T.F.G. Green, J.R. Yates, D. Massiot, Elucidation of the Al/Si ordering in gehlenite $Ca_2Al_2SiO_7$ by combined ^{29}Si and ^{27}Al NMR spectroscopy/quantum chemical calculations, Chem. Mater. 24 (2012) 4068–4079, https://doi.org/10.1021/cm3016935.

[38] R.D. Shannon, Revised effective ionic radii and systematic studies of interatomic distances in halides and chalcogenides, Acta Crystallogr. A32 (1976) 751–767, https://doi.org/10.1107/S0567739476001551.

[39] M.M. Kuklja, Defects in yttrium aluminium perovskite and garnet crystals: atomistic study, J. Phys. Condens. Matter 12 (2000) 2953–2967, https://doi.org/10.1088/0953-8984/12/13/307.

[40] A.P. Patel, M.R. Levy, R.W. Grimes, R.M. Gaume, R.S. Frigelson, K.J. McClellan, C. R. Stanek, Mechanisms of nonstoichiometry in $Y_3Al_5O_{12}$, Appl. Phys. Lett. 93 (2008), https://doi.org/10.1063/1.3002303, 191902-191902-3.

[41] J. Dong, K. Lu, Noncubic symmetry in garnet structures studied using extended X-ray-absorption fine-structure spectra, Phys. Rev. B 43 (1991) 8808–8821, https://doi.org/10.1103/PhysRevB.43.8808.

[42] N. Basavaraju, K.R. Priolkar, D. Gourier, S.K. Sharma, A. Bessière, B. Viana, The importance of inversion disorder in the visible light induced persistent luminescence in Cr^{3+} doped AB_2O_4 (A = Zn or Mg and B = Ga or Al), Phys. Chem. Chem. Phys. 17 (2015) 1790–1799, https://doi.org/10.1039/C4CP03866E.

[43] N. Yuan, X. Liu, F. Meng, D. Zhou, J. Meng, First-principles study of La_2CoMnO_6: a promising cathode material for intermediate-temperature solid oxide fuel cells due to intrinsic Co-Mn cation disorder, Ionics 21 (2015) 1675–1681, https://doi.org/10.1007/s11581-014-1320-z.

[44] M.S. Holston, J.W. McClory, N.C. Giles, L.E. Halliburton, Radiation-induced defects in $LiAlO_2$ crystals: holes trapped by lithium vacancies and their role in thermoluminescence, J. Lumin. 160 (2015) 43–49, https://doi.org/10.1016/j.jlumin.2014.11.018.

[45] W.B. Williamson, J.H. Lunsford, C. Naccahe, The EPR spectrum of O^- on magnesium oxide, Chem. Phys. Lett. 9 (1971) 33–34, https://doi.org/10.1016/0009-2614(71)80174-4.

[46] S.K. Misra, S.I. Andronenko, D. Tipkin, J.H. Freeman, V. Somani, O. Prakash, Study of paramagnetic defect centers in as-grown and annealed TiO_2 anatase and rutile nanoparticles by a variable-temperature X-band and high-frequency (236 GHz) EPR, J. Magn. Magn Mater. 401 (2016) 495–505, https://doi.org/10.1016/j.jmmm.2015.10.072.

[47] A. Ibarra, F.J. Lopez, J. Castro, V. centers, $MgAl_2O_4$ spinels, Phys. Rev. B 44 (1991) 7256, https://doi.org/10.1103/PhysRevB.44.7256.

[48] C.A. Hutchison, Paramagnetic resonance absorption in crystals colored by irradiation, Phys. Rev. 75 (1949) 1769–1770, https://doi.org/10.1103/PhysRev.75.1769.2.

[49] J.E. Wertz, P. Auzins, R.A. Weeks, R.H. Silsbee, Centers in magnesium oxide; confirmation of the spin of magnesium-25, Phys. Rev. 107 (1957) 1535–1537, https://doi.org/10.1103/PhysRev.107.1535.

[50] W.C. Holton, H. Blum, Paramagnetic resonance of F centers in alkali halide, Phys. Rev. 125 (1962) 89–103, https://doi.org/10.1103/PhysRev.125.89.

[51] A.J. Tench, R.L. Nelson, Electron spin resonance of F centres in irradiated ^{43}CaO and other alkaline earth oxides, Proc. Phys. Soc. 92 (1967) 1055, https://doi.org/10.1088/0370-1328/92/4/328.

[52] T. Kunio, H. Hitoshi, T. Hiroshi, ESR of F center in HgI_2·2HgS darkened with sunlight, Bull. Chem. Soc. Jpn. 50 (1977) 1341–1342, https://doi.org/10.1246/bcsj.50.1341.